Changes in cellular ferritin distribution in the human brain during autolysis revealed using analytical electron microscopy

Sowmya Sunkara[1], Snježana Radulović[1]*, Saška Lipovšek[1,2,3,4], Christoph Birkl[5], Stefan Eggenreich[6], Anna Maria Birkl-Toeglhofer[7], Maximilian Schinagl[1,8,10], Daniel Funk[1], Michael Stöger-Pollach[9], Johannes Haybaeck[7,10], Walter Goessler[11], Stefan Ropele[6], Gerd Leitinger[1]

[1]Gottfried Schatz Research Center, Division of Cell Biology, Histology and Embryology, Research Unit Electron Microscopic Techniques, Medical University of Graz, Graz, Austria
[2]Faculty of Medicine, University of Maribor, Maribor, Slovenia
[3]Department of Biology, Faculty of Natural Sciences and Mathematics, University of Maribor, Maribor, Slovenia
[4]Faculty of Chemistry and Chemical Engineering, University of Maribor, Maribor, Slovenia
[5]University Clinic for Neuroradiology, Medical University of Innsbruck, Innsbruck, Austria
[6]Neuroimaging Research Unit, Department of Neurology, Medical University of Graz, Austria
[7]Institute for Pathology, Neuropathology and Molecular Pathology, Medical University of Innsbruck, Innsbruck, Austria
[8]Institute of Chemical Technologies and Analytics, Technische Universität Wien, Vienna, Austria
[9]University Service Centre for Transmission Electron Microscopy (USTEM), Technische Universität Wien, Vienna, Austria
[10]Diagnostic & Research Center for Molecular BioMedicine, Institute of Pathology, Medical University of Graz, Graz, Austria
[11]Institute for Chemistry, University of Graz, Graz

*Correspondence: snjezana.radulovic@medunigraz.at

Abstract

Iron in the human brain is stored in the cores of ferritin proteins. Excess iron has been implicated in neurological disorders, so a careful balance of the iron concentration is thought to be essential for human health. Though it is known that oligodendrocytes contain most of the brain ferritin, followed by other glial cells

and neurons, changes in the number of filled ferritins or their cellular distribution during autolysis have not been revealed yet. To reveal these changes, we examined brain samples taken from six deceased humans at different *post-mortem* times. To compare samples with different ferritin content, the samples included the frontal gray and frontal white matter, which store a low amount of iron, and the putamen and globus pallidus, which store a high amount of iron. We quantified the number of loaded ferritin cores from iron L – elemental maps obtained with energy-filtered transmission electron microscopy. We then validated this number to the iron concentrations determined using inductively coupled plasma mass spectrometry and quantitative magnetic resonance imaging. The more loaded ferritin cores we found in the tissues, the higher the proportion of ferritins found in neurons instead of glial cells, indicating that total ferritin load scales with the proportion of ferritin that is located in neurons. Second, we found a statistically significant correlation between the *post-mortem* interval (PMI) and the concentration of loaded ferritins and found that this concentration is highly dependent on the *post-mortem* interval: the longer the PMI, the lower the ferritin concentration found in a sample. Third, the higher the total ferritin load, the higher the proportion of ferritins found in neurons instead of glial cells, indicating that ferritin loss during autolysis affects neurons and glial cells at different rates.

Key Words

Ferritin, human brain, energy-filtered transmission electron microscopy, quantitative magnetic resonance imaging, inductively coupled plasma mass spectrometry, frontal gray matter, frontal white matter, putamen, globus pallidus, autolysis, *post-mortem*.

Introduction

Non-heme iron accumulates in the normal ageing brain until the fourth decade of life [9]. The accumulation rates and the absolute iron concentration vary strongly across different brain regions: the highest concentrations can be found in the basal ganglia including the putamen and the globus pallidus (GP) [9, 16]. The cause of iron accumulation is still unclear, in particular since much more iron is stored than metabolically relevant.

Basal levels of iron are essential in an array of functions in the brain: e.g. myelin synthesis, acting as cofactors for enzymatic reactions [2], and synaptic plasticity [22]. However, high levels of soluble, free iron induce increased reactive oxygen species (ROS) levels [7, 10]. Labile iron ions can act as free radicals and can lead to neuroferritinopathy followed by neurodegeneration [7]. In the normal functioning brain, excess iron that is unused in the brain is stored in its storage protein, ferritin [34], thus protecting the brain from potential iron toxicity.

Ferritin is the main iron storage protein in the brain [6] and is critical for brain functioning since it is central to the iron regulatory mechanism. Its buffering properties allow it to store and release iron upon cellular demand, which is crucial in the prevention of ferroptosis (apoptosis induced by iron overload) [14] and other detrimental effects caused by free iron. Ferritin contains between 500 to 5000 ferric iron atoms in its inner core [11–13]. The size of the ferritin core in electron micrographs varies depending on various factors such as ferritin load, contrasting agent, hydration, or the focus of the electron micrograph. Previously published sizes range from 5.3 to 11 nm [12]. While the concentration of total

iron and ferritin-bound iron differs between brain areas, the size of ferritin cores remains largely uniform [7].

Ferritin takes a unique position amongst the iron-binding proteins, concerning its size and cargo capacity. Other iron-containing proteins like transferrin, and haemoglobin contain respectively only 2 or 4 iron atoms [8, 20, 33], so they are under the detection threshold for energy-filtered transmission electron microscopy, our method of choice for ferritin detection. On the other hand, hemosiderin is composed of conglomerates of clumped ferritin particles, denatured proteins, and lipids with a size up to 1 - 2 µm [33]. Accordingly, hemosiderin can be easily distinguished by size from ferritin but is rarely detected in the normal brain.

Post-mortem studies have the advantage that the tissue is available for a variety of measurements and procedures, including destructive ones. But autolysis sets off immediately after death, causing a breakdown of cells and tissues, changing structural components, and making it difficult to identify them [31], as reviewed in [18].

The total iron concentration in freeze-dried tissue samples can be determined most precisely by inductively coupled plasma mass spectrometry (ICP-MS), e.g. in reference [16]. However, this method is destructive. A non-invasive and thus non-destructive way to measure spatial iron concentrations is quantitative Magnetic Resonance Imaging (qMRI). qMRI allows to mapping the local transverse relaxation rate R_2*, which has been validated as a measure for iron content in brain tissue using ICP-MS [17]. However, neither method provides information on the amount of iron stored in ferritins or on its cellular distribution.

In this study we analyzed human brain samples *post-mortem* to answer two fundamental questions: first, we hypothesized that iron accumulation and cellular ferritin distribution change with *post-mortem* time. Second, we aimed to reveal the role of different cell types in preserving ferritin during autolysis. For this, we determined the ferritin concentration in human brain samples using analytical electron microscopy (EM). This procedure allowed us to visualize the chemical elements within thin tissue sections.

Further, we related results from analytical electron microscopy to qMRI and ICP-MS measurements of the iron content to obtain complementary insights into the effects of sensitivity and autolysis.

Materials and methods

Sampling

The samples used here are collected from six deceased human subjects who had to undergo routine brain autopsy at the Diagnostic and Research Institute of Pathology of the University Hospital Graz (approved by the Ethics Committee of the Medical University of Graz, votum number 28-549 ex 15/16). The subjects had not suffered from a known neurological disorder. To ensure that the analyses were not confounded by age, the specimen was collected from patients with ages ranging from 61- 86. At this age saturation in iron accumulation has already been reached [9]. The age and *post-mortem* intervals are given in Table 1. One-half of the brain was preserved for quantitative magnetic resonance imaging (qMRI) while four brain areas were dissected out of the other half and further divided

into samples for EFTEM and ICP-MS. The brain regions selected included two regions with the lowest iron concentrations - the frontal gray matter (FGM), the superficial frontal white matter (FWM), and two regions with higher concentrations of iron - the putamen, and the globus pallidus (GP) [1, 29, 35]. As soon as the tissue was cleared for research purposes by the pathologists, samples were dissected out and either immersed in fixative for EM, or placed into a plastic tube, weighed, and frozen for ICP-MS. The brain hemisphere for qMRI remained unfixed.

Table 1. Patient information

Patient code	Age [years]	PMI [h]
1	73	06:30
2	72	9
3	61	16
4	69	18
5	86	20
6	81	24

Electron Microscopy

Following the autopsy, 6-10 sub-samples of approximate wet weight 0.1-0.2 g (maximum dimensions 1x1x1 mm^3) were cut out of the samples and immersed in chemical fixative containing 2% formaldehyde, 2% glutaraldehyde in 0.1 M sodium cacodylate buffer. After fixation the samples were rinsed in the same buffer, postfixed in 1 % osmium tetroxide solution in the same buffer, dehydrated in a graded series of alcohols, immersed in propylene oxide, and embedded in TAAB embedding resin (TAAB, Aldermaston, UK). After curing for 3 days at

60 °C, thin sections were cut using a Leica UC6 or a Leica UC7 ultramicrotome at a thickness of either 60 or 70 nm. The sections were contrasted using platinum blue and lead citrate solutions. One block was randomly selected from each brain area for imaging and elemental mapping.

EM was performed with a Thermo Fisher Tecnai G2 20 electron microscope operated at 200 keV. An Ametek Gatan Quantum GIF energy filter with Ametek Gatan Ultrascan 1000 XP camera was used for energy-filtered transmission electron microscopy (EFTEM), and a bottom-mounted Ametek Gatan Ultrascan 1000 camera for bright field imaging. For elemental mapping, three windows – Pre-edge 1, Pre-edge 2, and Post-edge – were made at 80000x magnification, a binning of 2, a slot width of 40 eV, and an exposure time of 30 s. The energy losses were: 718 eV for the iron L – post-edge window, and 633 and 673 eV for the two pre-edge windows. Drift correction was done manually, and both an iron L – elemental map and an iron L – jump-ratio were computed on Digital Micrograph (Gatan, Inc) using respectively the three-window method and the two-window method.

An unbiased sampling protocol described earlier [15, 36] allowed us to automatically move each sample to 60 locations determined using a random number generator. The elemental maps were accompanied by overview micrographs taken from the same locations using the bright field mode at 3500x magnification.

Quantitating the number of ferritins and assessing cell types

Four independent researchers (SS, SnR, SL, and GL) each counted the number of iron-loaded ferritins and assessed the cell types. Ferritins were only counted if they were clearly visible as a bright spot on both the iron L – jump-ratio and the iron L – elemental maps and if at least three of the four researchers agreed on their number (otherwise images were analyzed again and all researchers counted ferritins simultaneously). If the number of ferritins exceeded 20 in any map, the mean value of the counts from four researchers was considered as the final count. Cell types were identified on the bright-field images and only noted if three of the four researchers agreed. For cell identification, the criteria described by [23]and the Boston University web atlas https://www.bu.edu/agingbrain/ (download 2022-01-14) were used. A total of 1440 iron L – elemental maps and 1440 iron L – jump ratios were generated and used for this study.

Quantitative Magnetic Resonance Imaging

MR imaging of the extracted brain hemisphere was performed using a 3.0 Tesla scanner (MAGNETOM PRISMA, Siemens Healthineers, Erlangen, Germany). A phased array head coil with 20 elements was used. For acquiring R_2* relaxation data, a two-dimensional radiofrequency-spoiled multi-echo gradient-echo sequence with 6 equally spaced echoes was applied (repetition time = 1150 ms, first echo time = 4.92 ms, echo spacing = 5.42 ms, flip angle = 15°; field of view = 256 x 256 mm^2 ; in-plane resolution = 0.75 x 0.75 mm^2 ; 2.4-mm-thick sections covering the entire hemisphere). Generalized autocalibrating partially parallel acquisition (GRAPPA) was performed with an acceleration factor of 2.
To reduce phase dispersion effects and to increase B0 homogeneity, second-order shimming was applied. R_2* maps were calculated with the relaxometry toolbox ((ESMRMB 2016, 33rd Annual Scientific Meeting, Vienna, AT, September 29 -

October 1: ePoster / Paper Poster / Clinical Review Poster / Software Exhibits 2016).

Inductively Coupled Plasma Mass spectrometry

All solutions were prepared with ultrapure water (18.2 MΩ*cm, Merck Millipore, Bedford, USA). Nitric acid (>65 % p.a.) was further purified via sub-boiling. For quantification, single elements standards (ROTI®Star, Carl Roth GmbH + Co. KG, Karlsruhe, Germany) were used.

Brain tissue was freeze-dried to constant mass with a Gamma 1-16 LSC freeze-dryer (Martin Christ GmbH, Osterode am Harz, Germany) and the wet/dry mass ratio was determined. Freeze-dried samples were weighed to 0.1 mg into the 12 mL quartz vessels of a microwave-heated autoclave, UltraCLAVE IV (EMLS, Leutkirch, Germany). After the addition of 3 mL subboiled nitric acid and 2 mL of water the quartz vessels were placed in the 40 positions rack of the autoclave and the autoclave was pressurized with Argon to a pressure of $4*10^6$ Pa. The following microwave heating program was applied: from room temperature to 80°C in 5 minutes, from

80°C to 150°C in 15 minutes, from 150°C to 250°C in 20 minutes, and 250°C for 30 minutes. After cooling to 80°C, the pressure was released and the samples were transferred to 50 mL polypropylene tubes (CELLSTAR®, blue screw cap, Greiner Bio-One GmbH, Kremsmuenster, Austria) and filled to the mark.

For the quantification of iron (Fecalibration curves were prepared from 0.0100 to 10.0 (Mg, Ca, Fe). Germanium (Ge) at a concentration of 200 µg/L was added as an internal standard online before the nebulizer. The samples were pumped through a peristaltic pump tubing with an i.d. of 1.05 mm and the internal

standard with a tubing of 0.19 mm. The elemental iron was quantified with an inductively coupled plasma mass spectrometer (ICP-MS, Agilent 7700x, Agilent Technologies, Waldbronn, Germany) at a mass-to-charge ratio of Fe m/z = 56. All isotopes were measured in the collision mode using He at a flow rate of 5.0 ml/min. The determined concentrations were calculated for fresh tissue.

The accuracy of the determined concentrations was confirmed with the certified material bovine muscle (RM 8414; NIST; now BOVM-1 NRCC).

Statistical Analysis and Graphs

Statistics were done using GraphPadPrism 9.2.0. One-way ANOVA with a Tukey's multiple comparisons test was used for statistical analysis with * $p < 0.05$; *** $p < 0.001$; **** $p < 0.0001$ for figures 2,3,5 and 8. For all comparison plots of data from three methodological approaches in figures 6, 7, and 9, a simple linear correlation analysis was performed.

Results

EFTEM elemental mapping allows visualizing ferritins cores in human *post-mortem* brain tissue

To visualize ferritin cores in electron micrographs, we made iron L – elemental maps and iron L – jump-ratios of brain samples for four different brain areas in each of six different deceased subjects. The maps consistently exhibited ferritins as bright spots of 5-10 nanometers in diameter (Fig. 1A-D). The size of the spots corresponded to the published sizes of ferritin cores [12], indicating that iron-filled ferritin cores could be visualized.

Ferritin cores were clustered in distinct cells

We next counted the number of ferritin cores in samples taken from the frontal cortex, the frontal white matter, the putamen, and the globus pallidus of each patient. The counts were made within 60 micrographs of 556 x 556 nm^2 dimensions and showed that the ferritins were not evenly distributed but clustered in certain micrographs (Fig. 2). We observed that the majority of ferritin accumulated as clusters as shown in figure 1, in the cells. At closer examination, it became apparent that certain cells accumulated ferritins, whereas others, often neighbouring cells, did not accumulate ferritins (Fig. 1). None of the ferritins appeared to be extracellular. We were able to assess the cell type (neuron, oligodendrocyte, astrocyte, or other unidentified glial cells) in 2,195 (62 %) of the 3,537 ferritin cores that we had identified in five out of six samples. 471 additional ferritin cores were identified in the sixth sample with a *post-mortem* interval of 24 h, but in this sample autolysis had progressed considerably, preventing us from faithfully identifying cell types. Accordingly, this sample was excluded from cell type identification experiments.

Ferritins accumulate in the putamen and globus pallidus

We next calculated the number of ferritins per μm^3 from the micrographs' 3D dimensions. Plotting this ferritin concentration in each brain region for each deceased person revealed that either the putamen, the globus pallidus, or both, had a significantly higher concentration of ferritins than either the frontal gray matter or the frontal white matter in five out of six patients (Fig. 3). Further, between the putamen and globus pallidus (4 out of 6 patients) significant differences were found (Fig. 3). The putamen had a significantly higher ferritin concentration than the globus pallidus in one out of six patients, and the globus

pallidus had a significantly higher concentration compared to the putamen in three out of six patients (Fig. 3).

qMRI and ICP-MS data support the EFTEM data

The ferritin concentrations counted from elemental maps were compared with the mean iron concentrations. The latter was determined by both mass spectrometry in adjacent tissue samples and by the proton transverse relaxation rate R_2* – a qMRI measure proportional to the iron concentration – measured in the contralateral hemisphere (Fig. 4). Each of the three methodological approaches provided higher mean values (of all the six samples) in the putamen and globus pallidus when compared to the frontal gray and frontal white matter (Fig. 5A–C)). Quantitative magnetic resonance imaging revealed a significant R_2* increase in putamen and globus pallidus compared to frontal white and frontal gray matter (Fig. 5B). Significant differences were found in the iron concentrations between the putamen and frontal gray matter using mass spectrometry (Fig. 5C).

To compare the three different methodological approaches, the mean values of the measured brain regions from all six deceased persons were correlated with each other. There was a high correlation between qMRI and ICP-MS results, each measuring the iron concentration. The higher the R_2* value, the higher the iron concentration (Fig. 6A, slope differs significantly from 0). However, we found no correlation between qMRI data and the mean ferritin count obtained using EFTEM (Fig. 6B), nor between the iron concentration by ICP-MS and mean ferritin count (Fig. 6C). This apparent discrepancy prompted us to check whether the *post-mortem* interval had an influence on the ferritin count or its cellular distribution.

The *post-mortem* interval influenced the mean ferritin count

We next tested whether putative autolysis during the *post-mortem* interval influenced the iron concentration, the storage of iron in ferritins, or the cellular distribution of the ferritins.

Our analysis showed that the mean ferritin count was inversely correlated to the *post-mortem* interval (Fig. 7A). In contrast, neither the R_2* value nor the ICP-MS determined iron concentration correlated with the *post-mortem* interval (Fig. 7B, C).

Cell type identification shows that most ferritins are contained in glial cells, especially oligodendrocytes

The counted ferritin was assessed to different cell types by four independent researchers. The ferritin distribution in different cell types showed that most of the 2195 ferritin cores that could be assigned to a specific cell type were found within glial cells. Oligodendrocytes represented the major cell type within this fraction (59 %). 17 % were found in neurons, 8% in astrocytes, and 1.7% in microglial cells (Fig. 8).

The percentage of ferritin cores found in neurons varies with both the PMI and the total ferritin count

Further, the percentage of ferritins found using EFTEM in neurons significantly decreased with increasing *post-mortem* interval (Fig. 9A). This indicates that the longer the *post-mortem* time, the lower the proportion of ferritins found in neurons and the higher the proportion of ferritins found in glial cells.

To evaluate whether the cell-specific accumulation of ferritin is dependent on the total ferritin amount, we plotted the percentage of ferritin found in neurons against the total ferritin count in each sample. Interestingly, this analysis showed that the percentage of ferritins stored in neurons increased with increasing ferritin count. In other words, when the ferritin concentration increases in a patient, the probability of ferritins accumulating in neurons increases. This result indicates that, although the majority of ferritins was situated in glial cells, total ferritin load scaled with the proportion of ferritins found in neurons compared to other cell types (Fig. 9B).

Discussion

In this study, we used analytical electron microscopy to determine the concentration of iron-loaded ferritin cores in the human brain. Thin sections taken from four brain regions of six deceased persons were examined. The persons had not suffered from a known neurological disorder and the samples were taken during routine autopsies. We aimed to assess the concentrations of local iron-loaded ferritin in the human brain during autolysis using EFTEM as the analytical electron microscopy method and then to validate our assessments with data on the R_2* relaxation rate obtained using qMRI (a marker for iron in brain tissue), and with the iron concentrations in neighbouring tissue samples obtained using ICP-MS.

Due to the electron density of the ferritins' iron cores, they are directly visible in classical electron micrographs (reviewed in [12]), but they can become obscured by the contrasting agent in routine contrasted sections [12]. Accordingly, we chose an energy filter to create iron maps for trustworthy ferritin core identification. The size [12] and detectability of these clusters indicate that they

correspond to the iron-loaded cores of ferritins. After identifying the ferritin cores, we compared the elemental maps with a classical electron micrograph of the same area for cell identification and ferritin localization. We were able to demonstrate that the putamen and the GP store more ferritin iron clusters than the FGM and the FWM, confirming a trend also seen in data obtained with both qMRI and ICP-MS.

It has to be borne in mind that the EFTEM method is based on visualizing iron clusters using analytical electron microscopy. Ferritins are known to vary in their iron load [11–13] and those ferritin proteins that contain a low amount of iron remain undetectable using EFTEM. Instead of using a fixed detection threshold, this study relied on four independent researchers agreeing on the ferritin count from both iron L – elemental maps and iron L – jump-ratios. There is high variability in the data obtained using the EFTEM method due to the small sampling size. Hence, the mean concentrations of ferritin both from each patient and each region were used for this study.

Although we have no means of counting empty ferritin molecules or ferritin molecules with a low iron load, we nevertheless were able to demonstrate that the putamen and globus pallidus had a higher mean concentration of detectable (iron-loaded) ferritins than the frontal gray and white matter. The basal ganglia as the storage site for iron have long been known [9] and have since been confirmed in several different studies that used a variety of different methods [16, 19, 26, 29]. To validate our findings, we measured the iron concentration in adjacent pieces of tissue taken from the same patients with ICP-MS, and measured the proton relaxation rate R_2*, using qMRI in the contralateral region of the same patients. Both methods were in good agreement and confirmed that the basal ganglia have both higher iron concentrations and a higher R_2*

relaxation rate than the frontal gray and white matter. This is also in line with an earlier study of *post-mortem* human brain tissue, in which qMRI was combined with ICP-MS to determine the relative iron concentrations within the tissue [17].

Our second aim was to reveal the role of different cell types in preserving ferritin during autolysis. We were able to determine the cell type (neuron, oligodendrocyte, astrocyte, or other glial cells) that contained most (86 %) of the ferritins we had detected in five out of the six patients. We found that most of the iron in the human brain is stored in oligodendrocytes, but iron is also found in other or unidentifiable glial cells and neurons. Owing to the fact that oligodendrocytes are the myelinating cells, it is apparent that more iron is stored in oligodendrocytes since it is used as a co-factor in lipid biosynthesis [5, 32]. Earlier studies support our results using a variety of different techniques [3, 21, 27, 28]. Interestingly, we found that the probability of the ferritins being stored in neurons rather than glial cells correlates positively with total ferritin concentration in each patient. To our knowledge, this is the first study that shows that total ferritin load scales with the proportion of ferritin that is located in neurons.

When plotting the mean R_2* relaxation rate against the mean iron concentration from gray matter structures of each patient, we found a high correlation between the R_2* relaxation rate and the absolute iron concentration, confirming an earlier, comparative study of both methods [16, 25]. In contrast, the mean ferritin concentration of all the brain areas did not correlate with the mean iron concentration of each patient, indicating that the number of loaded ferritins found in each patient was not directly dependent on the total iron concentration. This could be because the EFTEM method measures only those ferritin cores that are filled with a minimum threshold amount of iron, whereas both qMRI and ICMPS measure the total elemental iron load of the brain sample. We thus looked for a

factor that has an influence on the concentration of loaded ferritins and found that this concentration is highly dependent on the *post-mortem* interval: the longer the PMI, the fewer ferritins are found in a sample. This indicates that autolysis during the *post-mortem* time leads to either unloading or decay of ferritins. In contrast, neither the proton relaxation rate nor the total iron content was affected by the *post-mortem* interval. This signifies that the iron is not displaced during that interval, indicating that the proton relaxation rate represents the iron load of a specific brain area independent of the *post-mortem* interval. Further studies will be necessary to detect possible changes in the oxidation state during the unloading or decay of ferritins.

When looking into which cell types are involved in iron loss during the *post-mortem* interval, we again found that the loss occurs at a higher rate in neurons than in glial cells. Neurons were shown to have a different ferritin isoform distribution compared with glial cells [4, 24]. Moreover, when ferritin H (a subtype containing a high number of heavy chains) is selectively deleted in neurons, the protective effect of melatonin against ferroptosis is largely reduced [30] indicating that ferroptosis appears to be mainly driven by neurons. We thus can only speculate as to the cellular mechanisms that govern this loss of loaded ferritins during the *post-mortem* interval. Nevertheless, we have strong evidence that neurons are involved in it at a higher rate than glial cells.

In summary, we found high involvement of neurons in the storage of ferritins. Moreover, iron-loaded ferritins are lost *post-mortem*, in a yet unknown process, and loss of ferritins occurs at a higher rate in neurons than in glial cells.

Conclusion

We assessed the ferritin cores filled with iron in four different regions of the *post-mortem* brain using analytical electron microscopy. We established a relation between *post-mortem* interval, iron, and ferritin with emphasis on the role of different cells in ferritin storage. While we state that neurons store more ferritin with increasing ferritin count in each brain area, neurons are also depleted of ferritin *post-mortem* at a quicker rate compared to glial cells. We also demonstrate that the mean iron concentration is unaffected by *post-mortem* interval whereas ferritin concentration is. These findings pave way for studies on the cell-specific role in the storage of iron and its associated proteins during autolysis.

Acknowledgments

We are grateful to Dr. Sigurd Lax, for advice and for contributing material, Dr. Peter Simmons (Newcastle University, UK), for proofreading and language corrections, Mariella Sele, for processing the samples and for initially evaluating most of the samples, Elisabeth Bock, Elisabeth Pritz, Luca Schmid, Susanne Sumerauer and Nina Schlögl for expert technical assistance.

Abbreviations

EFTEM – energy-filtered transmission electron microscopy

EM – electron microscopy

FGM – frontal gray matter

FWM – frontal white matter

GP – globus pallidus

ICP-MS – inductively coupled plasma mass spectrometry

MR – magnetic resonance

PMI – *post-mortem* interval

qMRI – quantitative magnetic resonance imaging

Author contributions

SS, SnR, and GL planned and performed the experiments at the electron microscope, and computed elemental maps and jump ratios. SS, SnR, GL, and SL analyzed and quantified the raw data from elemental maps. JH, AMTB provided and assessed the brain tissue. StR, SE, and CB performed all qMRI experiments and analysis. WG performed ICP-MS experiments and analysis. PS proofread the manuscript. GL designed the project and study plan. All authors revised, read, and approved the manuscript.

Funding

This project was funded by the Austrian Science Foundation [FWF], grant P 29370.

Availability of data and material

Not applicable

Ethics approval and consent

The study design was approved by the Ethics Committee of the Medical University of Graz, votum number 28-549 ex 15/16.

Consent for publication

Not applicable

Competing interests

The authors declare no competing interests.

References

1. Bilgic B, Pfefferbaum A, Rohlfing T et al. (2012) MRI estimates of brain iron concentration in normal aging using quantitative susceptibility mapping. Neuroimage 59:2625–2635.
2. Codazzi F, Pelizzoni I, Zacchetti D et al. (2015) Iron entry in neurons and astrocytes: a link with synaptic activity. Front Mol Neurosci 8:18.
3. Connor JR, Menzies SL, St Martin SM et al. (1990) Cellular distribution of transferrin, ferritin, and iron in normal and aged human brains. J Neurosci Res 27:595–611.
4. Connor JR, Boeshore KL, Benkovic SA et al. (1994) Isoforms of ferritin have a specific cellular distribution in the brain. J Neurosci Res 37:461–465.
5. Connor JR, Menzies SL (1996) Relationship of iron to oligondendrocytes and myelination. Glia 17:83–93.
6. Finazzi D, Arosio P (2014) Biology of ferritin in mammals: an update on iron storage, oxidative damage and neurodegeneration. Arch Toxicol 88:1787–1802.

7. Friedman A, Arosio P, Finazzi D et al. (2011) Ferritin as an important player in neurodegeneration. Parkinsonism Relat Disord 17:423–430.
8. Giometto B, Gallo P, Tavolato B (1993) Transferrin Receptors in the Central Nervous System. In: Conn PM (ed) Methods in neurosciences, vol 11. Elsevier, pp 122–134
9. Hallgren B, Sourander P (1958) The effect of age on the non-haemin iron in the human brain. J Neurochem 3:41–51.
10. Halliwell B (2006) Oxidative stress and neurodegeneration: where are we now? J Neurochem 97:1634–1658.
11. Harrison PM, Arosio P (1996) The ferritins: molecular properties, iron storage function and cellular regulation. Biochimica et Biophysica Acta (BBA) - Bioenergetics 1275:161–203.
12. Iancu TC (2011) Ultrastructural aspects of iron storage, transport and metabolism. J Neural Transm (Vienna) 118:329–335.
13. Jian N, Dowle M, Horniblow RD et al. (2016) Morphology of the ferritin iron core by aberration corrected scanning transmission electron microscopy. Nanotechnology 27:46LT02.
14. Jiang X, Stockwell BR, Conrad M (2021) Ferroptosis: mechanisms, biology and role in disease. Nat Rev Mol Cell Biol 22:266–282.
15. JoVE Video Dataset
16. Krebs N, Langkammer C, Goessler W et al. (2014) Assessment of trace elements in human brain using inductively coupled plasma mass spectrometry. J Trace Elem Med Biol 28:1–7.
17. Langkammer C, Krebs N, Goessler W et al. (2010) Quantitative MR imaging of brain iron: a postmortem validation study. Radiology 257:455–462.

18. Lewis AJ, Genoud C, Pont M et al. (2019) Imaging of post-mortem human brain tissue using electron and X-ray microscopy. Curr Opin Struct Biol 58:138–148.
19. Maeda H, Sato M, Yoshikawa A et al. (1997) Brain MR imaging in patients with hepatic cirrhosis: relationship between high intensity signal in basal ganglia on T1-weighted images and elemental concentrations in brain. Neuroradiology 39:546–550.
20. Marengo-Rowe AJ (2006) Structure-function relations of human hemoglobins. Proc (Bayl Univ Med Cent) 19:239–245.
21. Meguro R, Asano Y, Odagiri S et al. (2008) Cellular and subcellular localizations of nonheme ferric and ferrous iron in the rat brain: a light and electron microscopic study by the perfusion-Perls and -Turnbull methods. Arch Histol Cytol 71:205–222.
22. Muñoz P, Humeres A, Elgueta C et al. (2011) Iron mediates N-methyl-D-aspartate receptor-dependent stimulation of calcium-induced pathways and hippocampal synaptic plasticity. J Biol Chem 286:13382–13392.
23. Nahirney PC, Tremblay M-E (2021) Brain Ultrastructure: Putting the Pieces Together. Front Cell Dev Biol 9:629503.
24. Nash B, Tarn K, Irollo E et al. (2019) Morphine-Induced Modulation of Endolysosomal Iron Mediates Upregulation of Ferritin Heavy Chain in Cortical Neurons. eNeuro 6.
25. Péran P, Cherubini A, Luccichenti G et al. (2009) Volume and iron content in basal ganglia and thalamus. Hum Brain Mapp 30:2667–2675.
26. Pfefferbaum A, Adalsteinsson E, Rohlfing T et al. (2009) MRI estimates of brain iron concentration in normal aging: comparison of field-dependent (FDRI) and phase (SWI) methods. Neuroimage 47:493–500.

27. Quintana C, Cowley JM, Marhic C (2004) Electron nanodiffraction and high-resolution electron microscopy studies of the structure and composition of physiological and pathological ferritin. J Struct Biol 147:166–178.
28. Quintana C, Bellefqih S, Laval JY et al. (2006) Study of the localization of iron, ferritin, and hemosiderin in Alzheimer's disease hippocampus by analytical microscopy at the subcellular level. J Struct Biol 153:42–54.
29. Ramos P, Santos A, Pinto NR et al. (2014) Iron levels in the human brain: a post-mortem study of anatomical region differences and age-related changes. J Trace Elem Med Biol 28:13–17.
30. Rui T, Wang H, Li Q et al. (2021) Deletion of ferritin H in neurons counteracts the protective effect of melatonin against traumatic brain injury-induced ferroptosis. J Pineal Res 70:e12704.
31. Sele M, Wernitznig S, Lipovšek S et al. (2019) Optimization of ultrastructural preservation of human brain for transmission electron microscopy after long post-mortem intervals. Acta Neuropathol Commun 7:144.
32. Todorich B, Pasquini JM, Garcia CI et al. (2009) Oligodendrocytes and myelination: the role of iron. Glia 57:467–478.
33. Wagner KR, Sharp FR, Ardizzone TD et al. (2003) Heme and iron metabolism: role in cerebral hemorrhage. J Cereb Blood Flow Metab 23:629–652.
34. Wang J, Pantopoulos K (2011) Regulation of cellular iron metabolism. Biochem J 434:365–381.
35. Ward RJ, Zucca FA, Duyn JH et al. (2014) The role of iron in brain ageing and neurodegenerative disorders. The Lancet Neurology 13:1045–1060.

36. Wernitznig S, Reichmann F, Sele M et al. (2019) An Unbiased Approach of Sampling TEM Sections in Neuroscience. J Vis Exp.

Table and figures

Table 1. Patient information

Figure 1. EFTEM mapping of iron in different regions in *post-mortem* human brain sample. (a) bright-field electron micrographs, (b) inverted post-edge micrographs, (c) iron L – jump-ratios, and (d) corresponding iron L - elemental maps of the same region as (b). (A) shows an overview image of the FGM region (B) the FWM region (C) the putamen region, and (D) the GP region. Ferritin filled with iron core appears as bright spots. Examples are marked by red arrows. Corresponding iron L – jump-ratios and iron L - elemental maps (c,d) show ferritin present in clusters in the cells.

Figure 2. The ferritin concentration in different brain regions varies between patients 1-6. (A) FGM. (B) FWM. (C) Putamen. (D) GP. Data are shown as bar graphs with whiskers representing the mean ± SEM. Each dot represents the ferritin concentration measured in one iron L - elemental map, (n = 60 for each patient in each brain region). One-way ANOVA with Tukey's multiple comparisons test was used.

Figure 3. The ferritin concentration is often, but not always, higher in the basal ganglia than in the frontal gray or frontal white matter. Graphs show the ferritin concentration in the FGM, FWM, putamen, and GP in (A) patient 1, (B) patient 2, (C) patient 3, (D) patient 4, (E) patient 5, and (F) patient 6. Data are shown as bar graphs with whiskers representing the mean ± SEM. Each dot represents the ferritin concentration measured in one iron L - elemental map, respectively (n =

60 for each brain region and each patient). One-way ANOVA with a Tukey's multiple comparisons test was used for statistical analysis with * $p < 0.05$; ** $p < 0.01$; **** $p < 0.0001$.

Figure 4. MRI scan showing an axial T_1-weighted image of (A) one cerebral hemisphere and (B) the corresponding R_2* map. The bright areas in (B) are the putamen and the globus pallidus with higher R_2* rates as a consequence of age-related iron accumulation.

Figure 5. The differences in ferritin concentration determined by EFTEM between brain areas follow the same trend as the sample from the counter brain half in qMRI data and adjacent samples in ICP-MS data. (A) Ferritin concentration in the FGM, FWM, putamen, and GP measured by EFTEM. (B) Iron concentration in the FGM, FWM, putamen, and GP measured by ICP-MS. (C) Proton transverse relaxation rate (R_2*) in the FGM, FWM, putamen, and GP measured by qMRI. Data are shown as bar graphs with whiskers representing the mean ± SEM. Each dot represents the mean ferritin concentration measured in one patient, respectively ($n = 6$). One-way ANOVA with a Tukey's multiple comparisons test was used for statistical analysis with * $p < 0.05$; *** $p < 0.001$; **** $p < 0.0001$.

Figure 6. Correlation between mean concentrations of ferritin and iron measured via EFTEM, qMRI, and ICP-MS respectively. (A) Proton transverse relaxation rate (qMRI) plotted over the iron concentration (ICP-MS) for each patient. The mean proton transverse relaxation rate of each patient correlates significantly with the mean iron concentration ($r^2 = 0.8560$). (B) Mean ferritin concentration (EFTEM) plotted over the proton transverse relaxation rate (R_2*) (qMRI). (C) Mean ferritin concentration (EFTEM) plotted over the iron concentration (ICP-MS). In contrast to A, the mean concentration of ferritin particles does not

correlate with proton relaxation rate (B, r^2 = 0.0230) nor with the iron concentration (C, r^2 = 0.0043). Each dot represents the mean ferritin concentration or the mean iron concentration measured in one patient, respectively (n = 6). Linear correlation analysis was used for statistical analysis with a level of significance of p = 0.0082 for A, p = 0.0230 for B, and p = 0.9015 for C. Plots are based on mean values of the FGM, FWM, the putamen, and the GP for all the plots.

Figure 7. Ferritin particles disintegrate and their concentration is reduced over time *post-mortem* time. (A) Mean values of the ferritin concentration (EFTEM) in all the brain regions plotted against PMI, r^2 = 0.6421. (B) Mean values of the proton transverse relaxation rate (qMRI) in all the brain regions plotted against PMI, r^2 = 0.1323. (C) Mean values of the iron concentration (ICP-MS) in all the brain regions. r^2 = 0.1215. The ferritin concentration decreases with PMI in regions of the brain (A) whereas the total iron load in the four regions of the brain does not seem to be influenced by the PMI (B, C). Each dot represents the mean ferritin concentration or the mean iron concentration measured in one patient, respectively (n = 6). Linear correlation analysis was used for statistical analysis with a level of significance of 0.0553 for A, 0.4785 for B, and 0.4983 for C. Plots are based on mean values of the FGM, FWM, the putamen, and the GP for all the plots.

Figure 8. Ferritin is predominately stored in glial cells (82 %) and especially in oligodendrocytes (59 %); followed by 8% in astrocytes and 1.7% in microglial cells of the identified glial cells. 19 % is stored in neurons. The graph shows those ferritin particles in the FGM, FWM, putamen, and GP of patients 1-5

whose cell type could be determined. One-way ANOVA with Tukey's multiple comparisons test was used for statistical analysis.

Figure 9. The percentage of ferritin in neurons varies with *post-mortem* time and with total ferritin concentration. (A) Percentage of ferritins in neurons from patients 1 to 5 plotted against PMI. Mean values of the percentage of ferritin concentration in neurons (EFTEM) reduce over time with increasing PMI, r^2 = 0.8338. (B) Mean values of the percentage of ferritins found in neurons in all brain regions from patients 1 to 5 were plotted against total ferritin count. The probability of ferritins being found in neurons rises with the total ferritin concentration, r^2 = 0.8227. Each dot represents the mean percentage of ferritin found in neurons in all brain regions measured in patients 1-5, respectively (n = 5). Linear correlation analysis was used for statistical analysis with a level of significance of p = 0.0303 for A and p = 0.0336 for B.

Figure 1

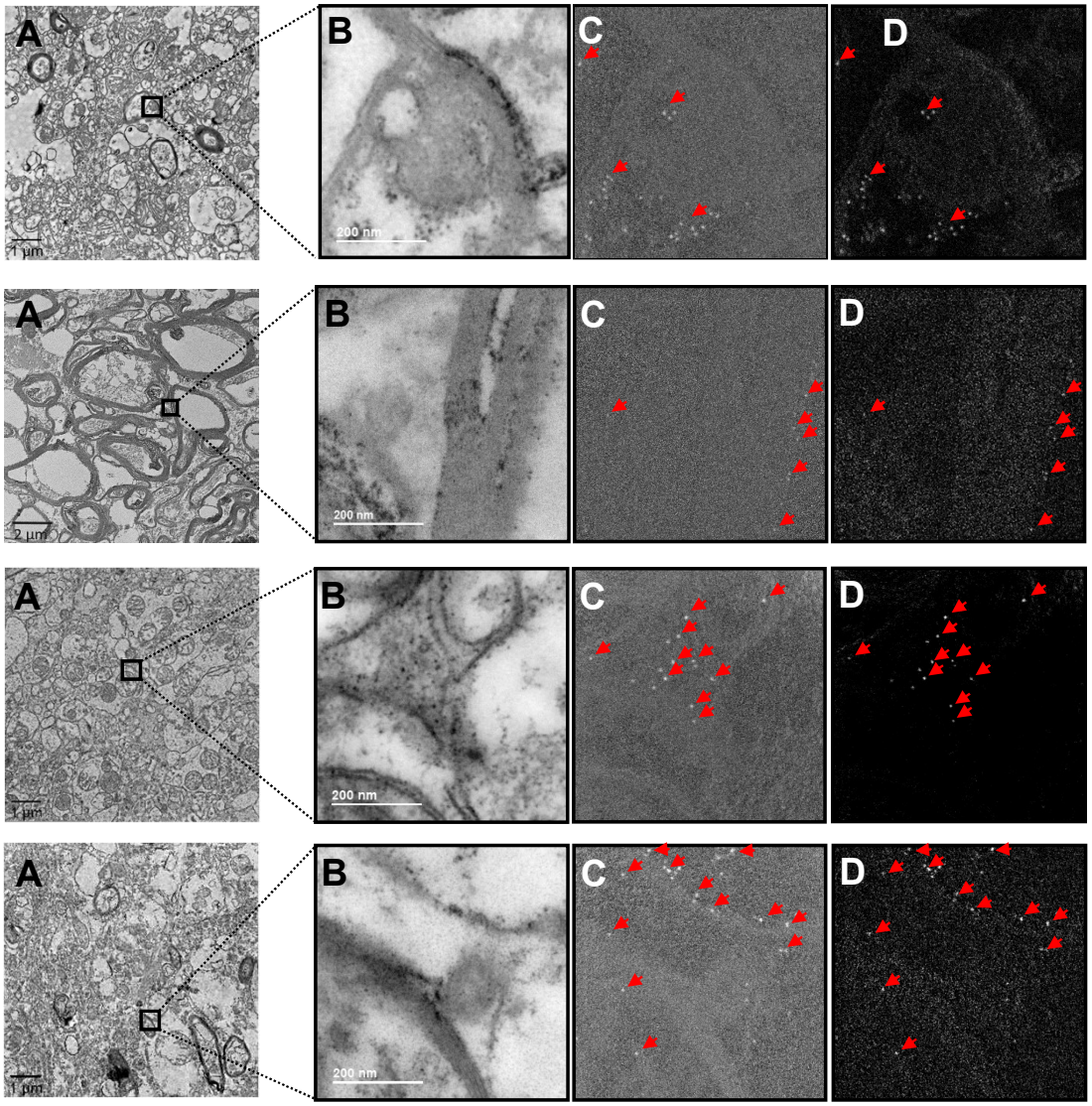

Figure 2

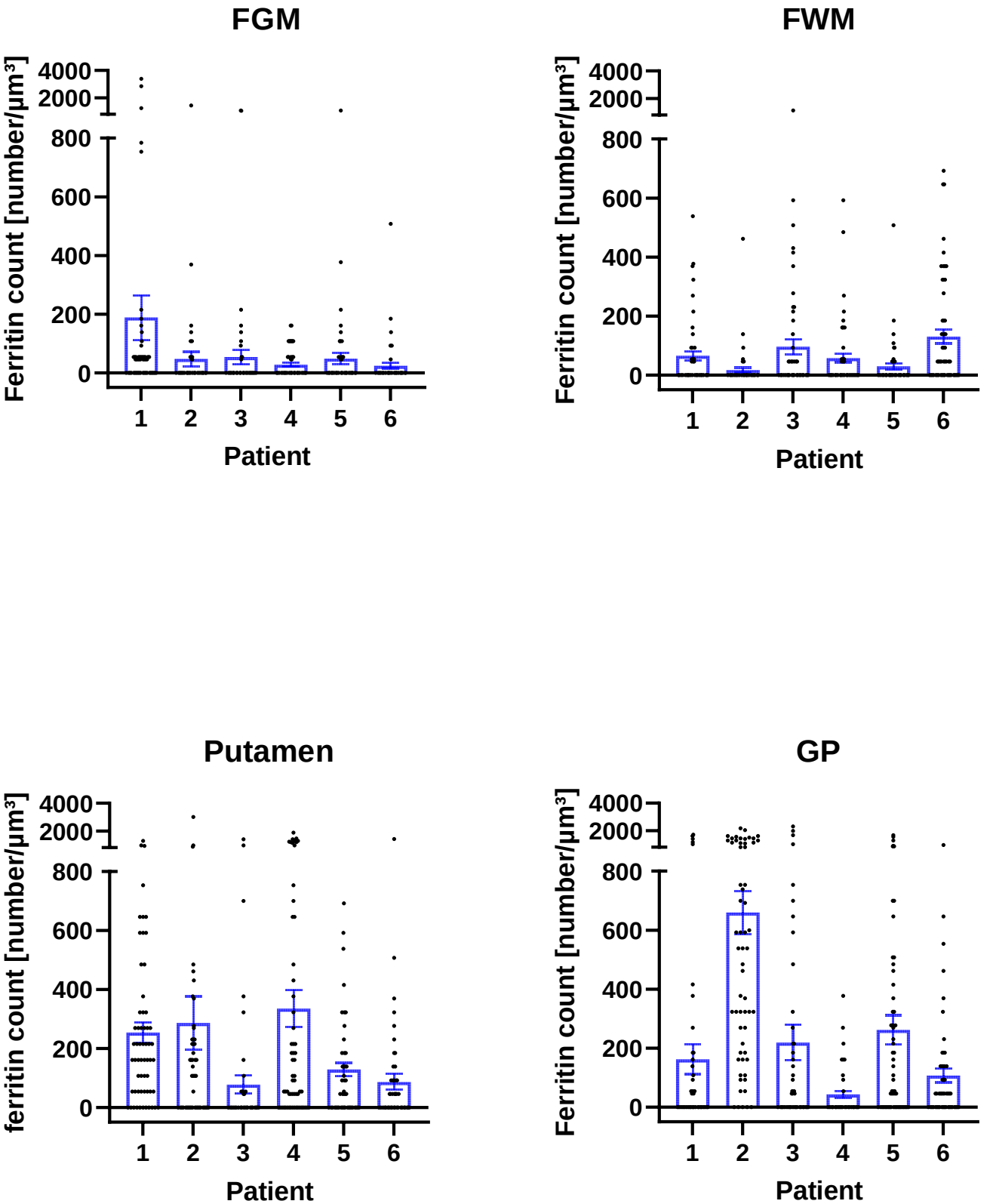
FGM
Ferritin count [number/µm³]
4000
2000
800
600
400
200
0
1
2
3
4
5
6
Patient
FWM
Ferritin count [number/µm³]
4000
2000
800
600
400
200
0
1
2
3
4
5
6
Patient
Putamen
ferritin count [number/µm³]
4000
2000
800
600
400
200
0
1
2
3
4
5
6
Patient
GP
Ferritin count [number/µm³]
4000
2000
800
600
400
200
0
1
2
3
4
5
6
Patient

Figure 3

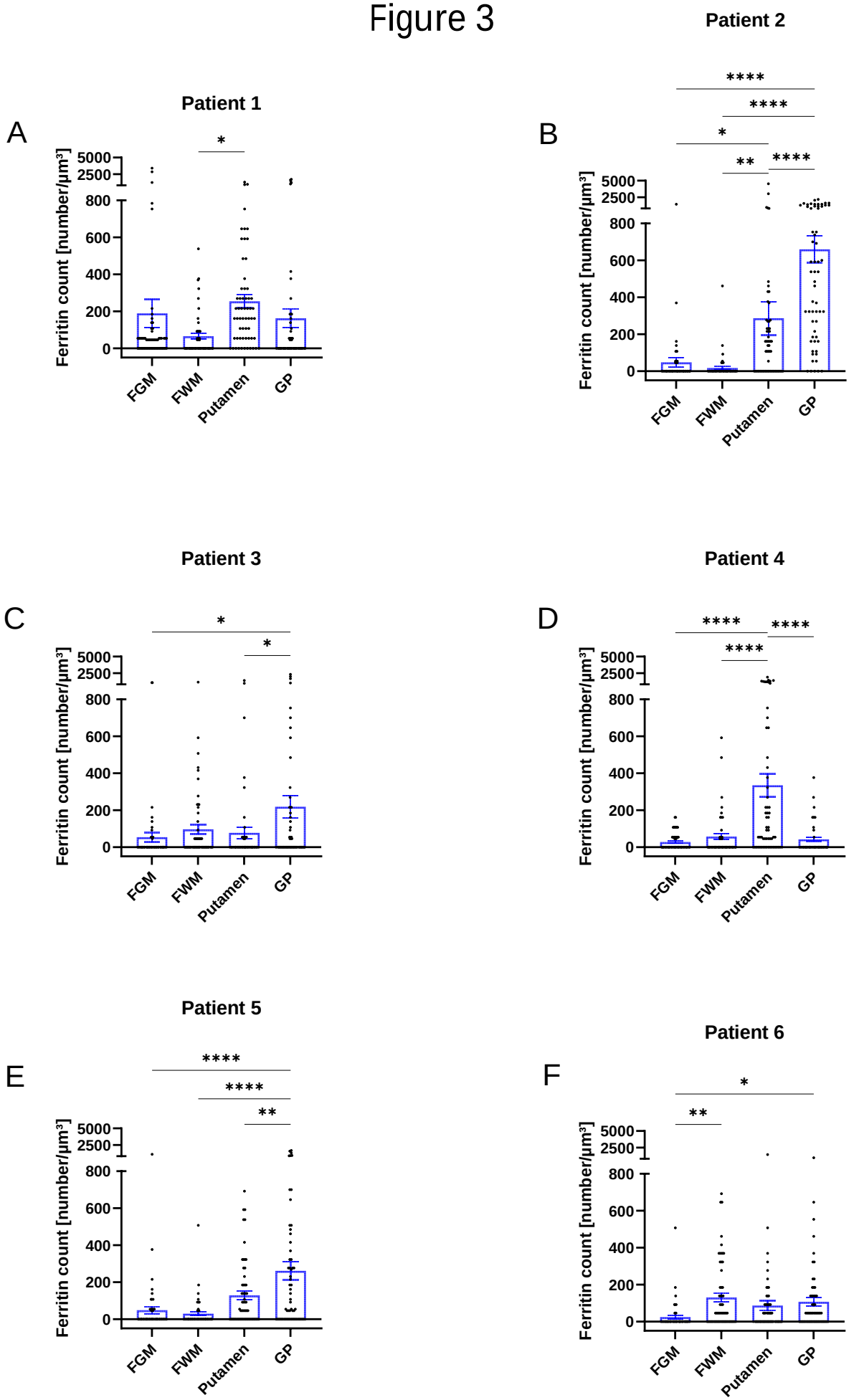
A
Patient 1
*
Ferritin count [number/µm³]
5000
2500
800
600
400
200
0
FGM
FWM
Putamen
GP
B
Patient 2
****
****
*
**
****
C
Patient 3
*
*
D
Patient 4
****
****
****
E
Patient 5
****
****
**
F
Patient 6
*
**

Figure 5

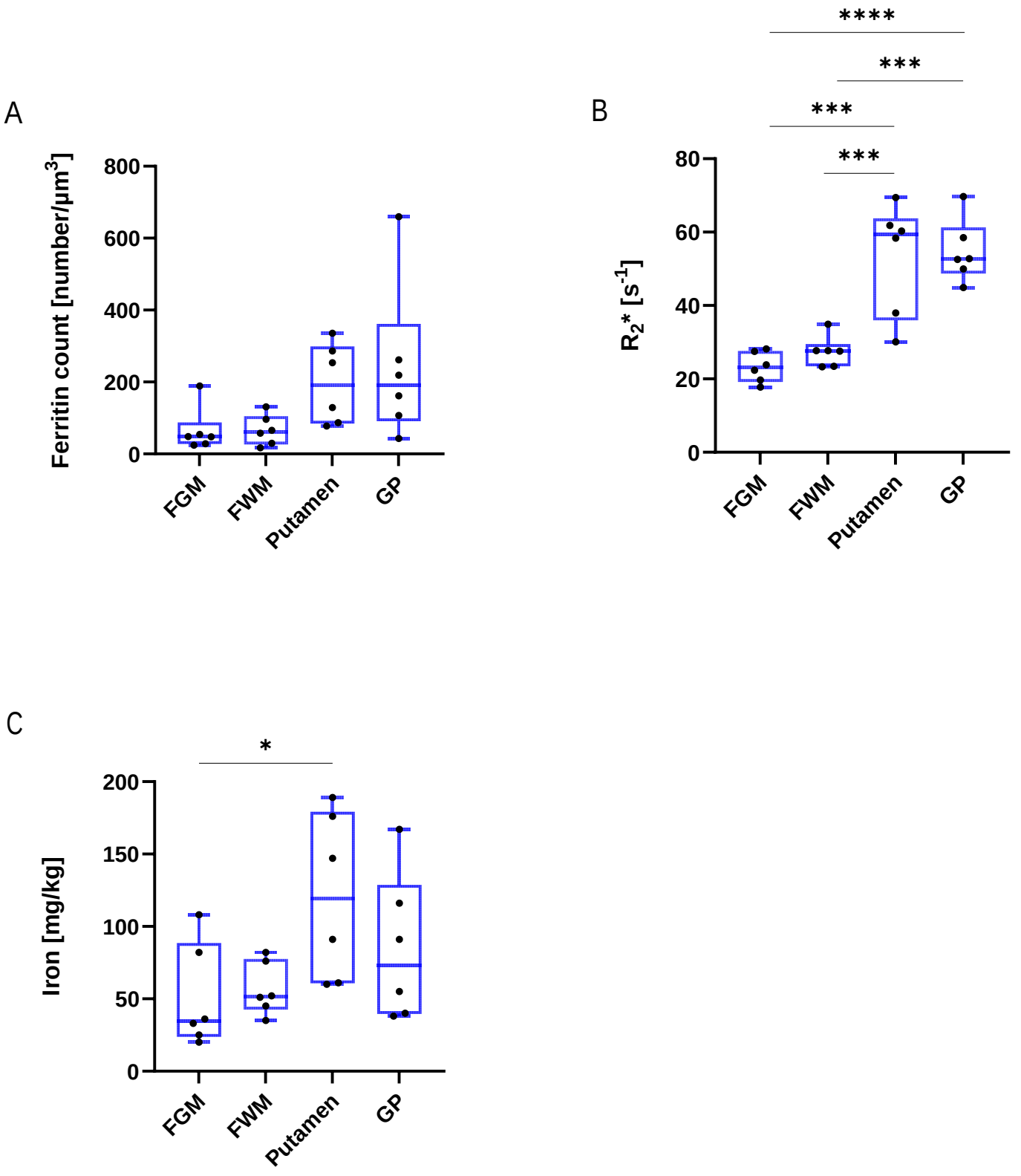
A
Ferritin count [number/µm³]
800
600
400
200
0
FGM
FWM
Putamen
GP
B
****
***
***
***
R₂* [s⁻¹]
80
60
40
20
0
FGM
FWM
Putamen
GP
C
*
Iron [mg/kg]
200
150
100
50
0
FGM
FWM
Putamen
GP

Figure 6

A

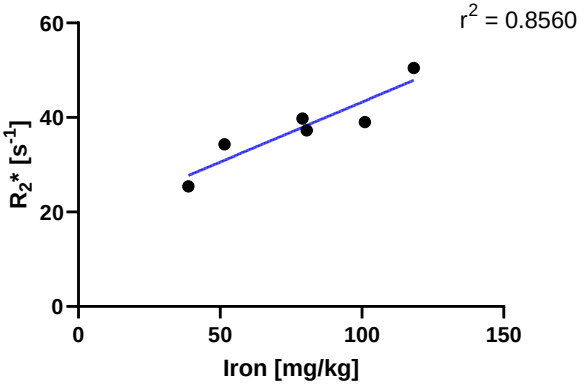
r2 = 0.8560
R2* [s-1]
60
40
20
0
0
50
100
150
Iron [mg/kg]

B

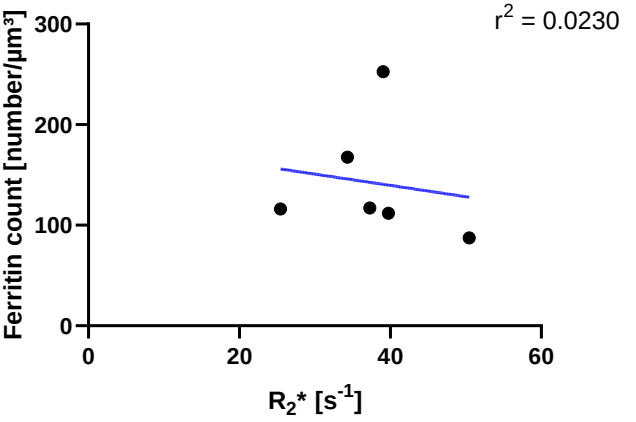
r2 = 0.0230
Ferritin count [number/µm³]
300
200
100
0
0
20
40
60
R2* [s-1]

C

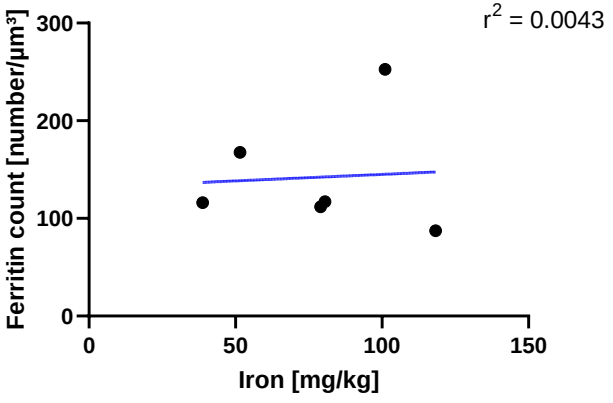
r2 = 0.0043
Ferritin count [number/µm³]
300
200
100
0
0
50
100
150
Iron [mg/kg]

Figure 7

A

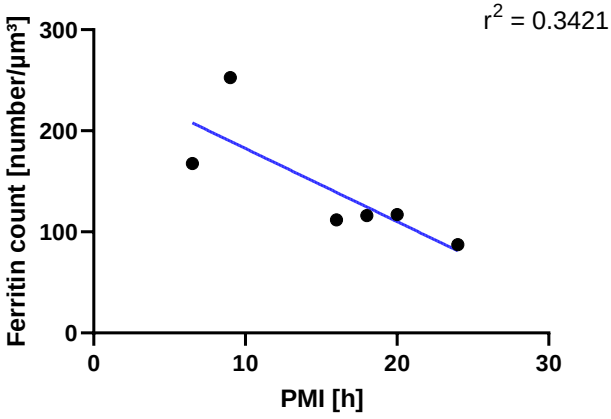
r2 = 0.3421
Ferritin count [number/µm³]
300
200
100
0
0
10
20
30
PMI [h]

B

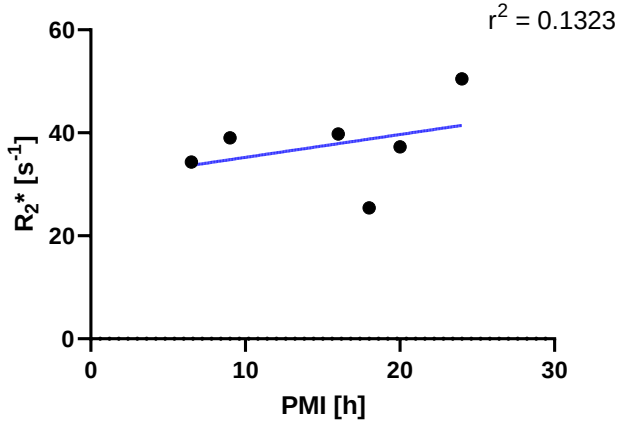
r2 = 0.1323
R2* [s-1]
60
40
20
0
0
10
20
30
PMI [h]

C

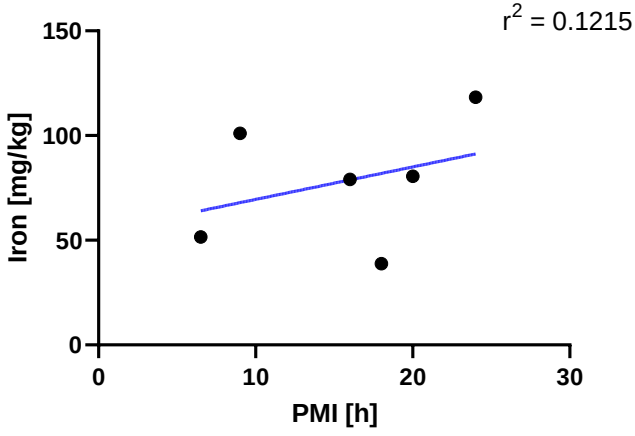
r2 = 0.1215
Iron [mg/kg]
150
100
50
0
0
10
20
30
PMI [h]

Figure 8

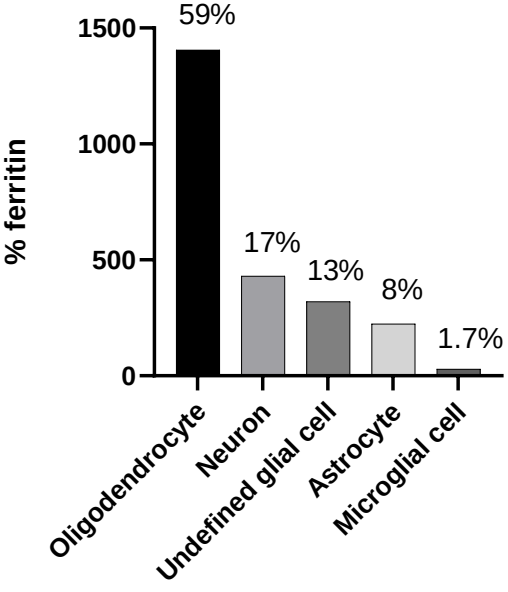
% ferritin
1500
1000
500
0
59%
17%
13%
8%
1.7%
Oligodendrocyte
Neuron
Undefined glial cell
Astrocyte
Microglial cell

Figure 9

A

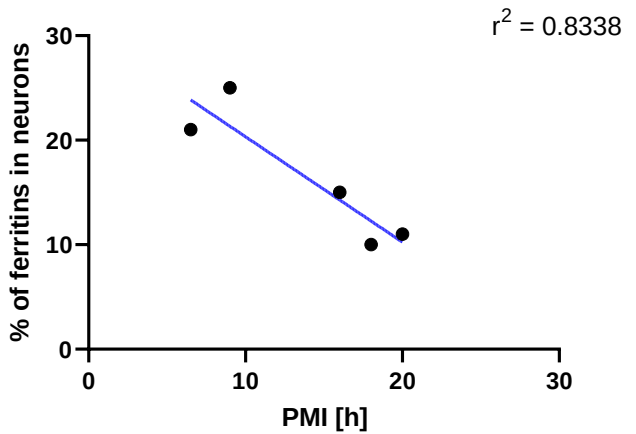
r2 = 0.8338
% of ferritins in neurons
30
20
10
0
0
10
20
30
PMI [h]

B

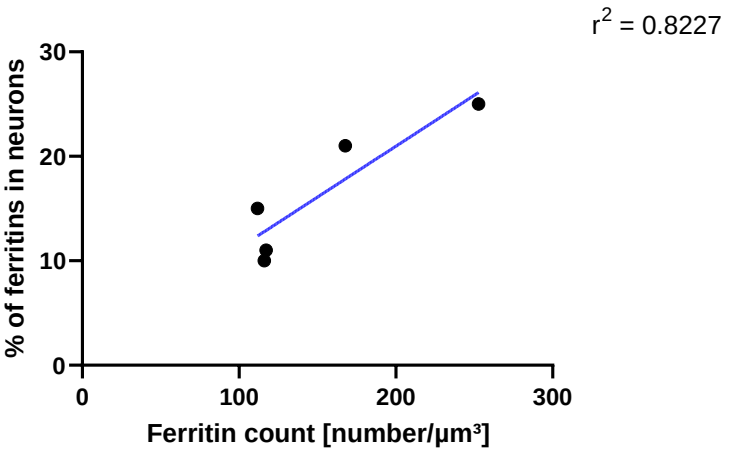
r2 = 0.8227
% of ferritins in neurons
30
20
10
0
0
100
200
300
Ferritin count [number/µm³]

A

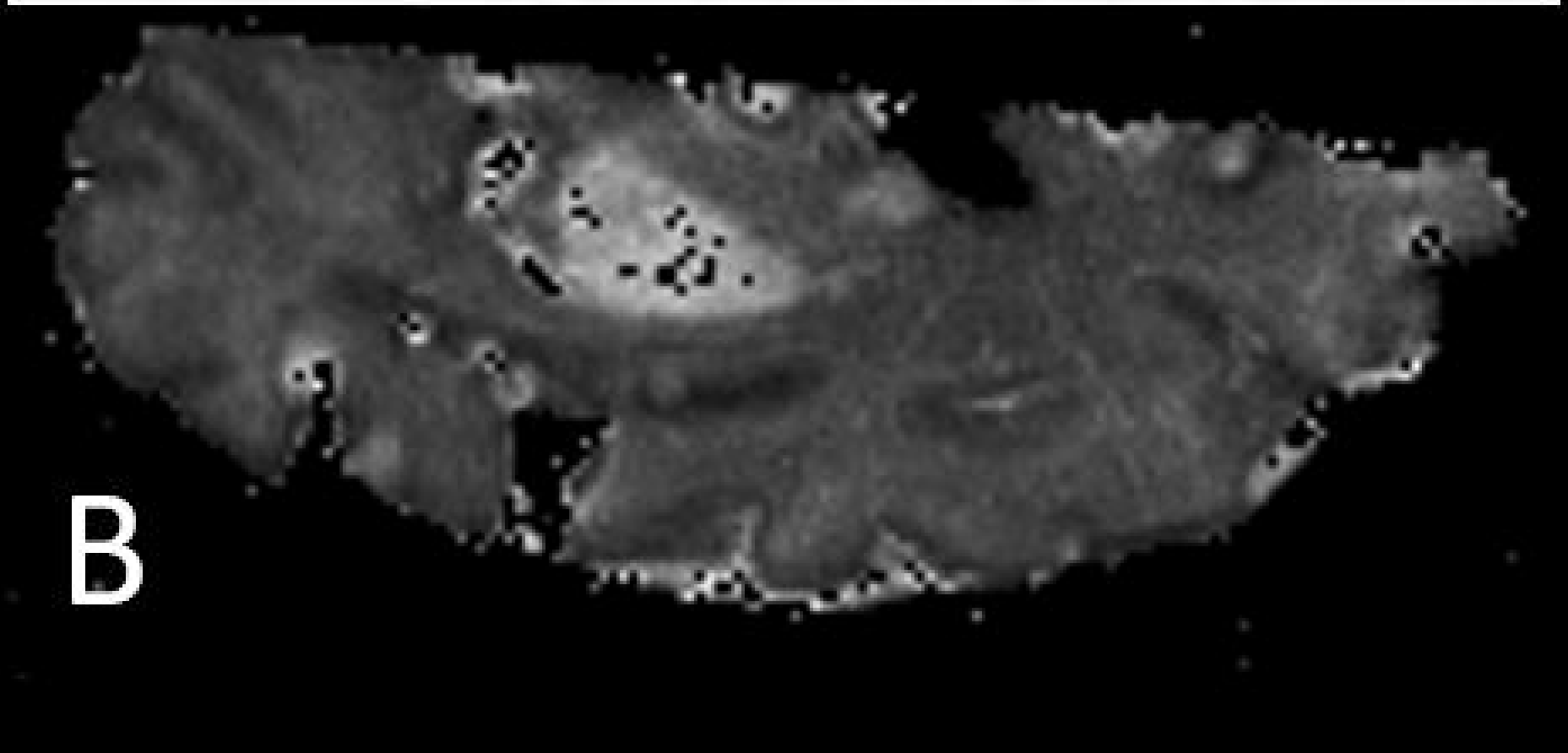
B